MICROSCOPIC OBSERVATION AND MODELING OF TOUGHENING MECHANISM IN RUBBER-MODIFIED POLYMER

M. Todo[1] and K. Arakawa[1]
[1]Research Institute for Applied Mechanics, Kyushu University, Kasuga, Fukuoka 816-8580, Japan

ABSTRACT

Toughening mechanisms of two different rubber-modified polymers, namely, rubber-toughened PMMA (RT-PMMA) and MBS resin, were investigated by transmission electron microscopy (TEM) and finite element analysis (FEA). The TEM result showed that in typical RT-PMMA, micro-craze formation in crack-tip region is the primary toughening mechanism. On the other hand, in a type of MBS, large plastic deformation of rubber particles and the surrounding matrix resin was observed in a limited area in the vicinity of crack-tip. FEA was performed to simulate these different types of damage mechanism in crack-tip region. For the damage formation in RT-PMMA, a damage model was applied to simulate damage zone formation in the crack-tip region in the macro-scale analysis and micro-crazing in the surroundings of rubber particles in the micro-scale model. It was shown that the damage model was successfully applied to predict these damage formations. For the plastic deformation in MBS, it was assumed that heat generation in the vicinity of crack-tip plays an important role in the formation of such large-scale deformation. Therefore, dynamic nonlinear FEM analysis was performed to analyze the heat generation in the crack-tip region. It was shown that the crack-tip temperature rose up to about 80°C, suggesting increase of ductility in the crack-tip region.

1 INTRODUCTION

Transparent thermoplastics, PMMA and MS, have widely been used in automobile, aerospace, optics, electronics and architecture industries. However, these plastics are brittle in nature, and many efforts have been made to improve their fracture toughness by blending small rubber particles with PMMA and MS matrices. Although the rubber-toughened plastics have already come into practical use, the details of the toughening mechanisms have not been elucidated yet. It is important to understand such mechanisms to develop new materials with higher performances. The toughening mechanisms are generally related to micro-damage formation in highly stressed region, and therefore, it is needed to apply microscopies in high resolution such as transparent electron microscopy. In addition to such experimental mechanics, computational mechanics may be a powerful tool to investigate complicated phenomena observed in the two-phase materials.

Our research group has been investigated the toughening mechanism of RT-PMMA, and it has been shown that the energy dissipation due to damage zone formation in the vicinity of crack-tip is the primary toughening mechanism in this kind of rubber toughened polymer [1,2]. It has also been shown that a crowd of micro-crazes generated in the surroundings of rubber particles form the damage zone. However, it is still unclear how the micro-crazes and damage zone initiate and grow. Fracture micro-mechanisms of variety kinds of MBS has also been studied, and it has been shown that the size and content of rubber particle and bimodal distribution play important roles in micro-damage formation in the crack-tip regions [3].

In this study, damage zone development was characterized using a compact tensile testing machine with an optical microscope and a digital camera. Nonlinear FEA with the aid of the damage model was performed to simulate the damage zone development by constructing a macro-scale model of the whole specimen geometry. A micro-scale model consisting of

distributing particles and matrix was constructed using a FE-SEM image of the microstructure. Then, FEA was performed to simulate micro-craze formation observed by TEM. Micro-scale deformation in a crack-tip region of a MBS resin containing nano-scale particles under impact loading was characterized by TEM. Dynamic nonlinear FEA was then performed to simulate heat generation in the crack-tip region to assess the plastic deformation mechanism presumed based on the TEM result.

2 DAMAGE-ZONE OBSERVATION

2.1 RT-PMMA

A RT-PMMA containing 20wt% butyl acrylate-co-styrene rubber was prepared to examine its toughening mechanism. The diameter of the distributing particles is about 300 nm, and they form a core-shell structure. Sheets of 0.21 mm thick was fabricated by a hot press from plates of 1.6 mm thick, and then, tensile specimens with single V-notches were processed. Mode I fracture tests of the specimens were conducted using a compact tensile testing machine, and the damage zone developments in the notch-tip regions were observed and recorded using a polarizing optical microscope (POM) and digital camera. Load-time and displacement-time relations were also recorded using a digital recorder.

A POM micrograph of damage zone generated at a maximum loading point is shown in Figure 1. It is observed that the damage zone forms cloud-like shape in the notch-tip region. A TEM micrograph of micro-crazing in a crack-tip region is shown in Figure 2. These micro-crazes appear to be formed in the direction perpendicular to the maximum principal stress. It is thus understood that the damage zone is created as a crowd of micro-crazes.

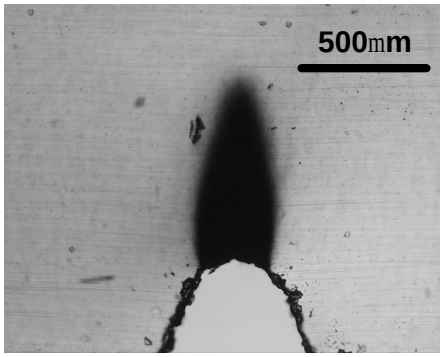

Figure 1: Damage zone development.

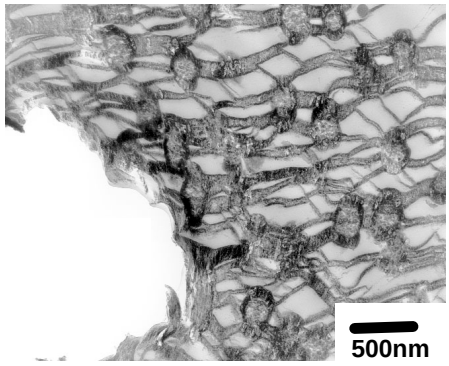

Figure 2: TEM micrograph of micro-crazing.

2.2 MBS resin

A MBS resin containing 10wt% nano-scale butadiene particles was prepared to examine its impact deformation mechanism. The average diameter of the rubber particles is 140 nm. Double-edge-notch-bend (DENB) specimens were processed from the MBS plates of 5mm thick. The geometry of the DENB specimen is shown in Figure 3. Four-point bend tests of the DENB specimens were carried out using an instrumented drop weight impact testing system at an impact loading rate of 1 m/s. For each of the impact tests, an arrested crack accompanied by damage zone formation was obtained. Thin sections of the damage zone regions were prepared using an ultra microtome after the specimens were stained by osmium oxide. Then, the thin samples were observed by a transmission electron microscope.

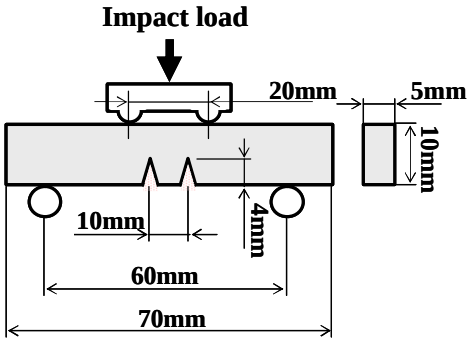

Figure 3: DENB specimen geometry.

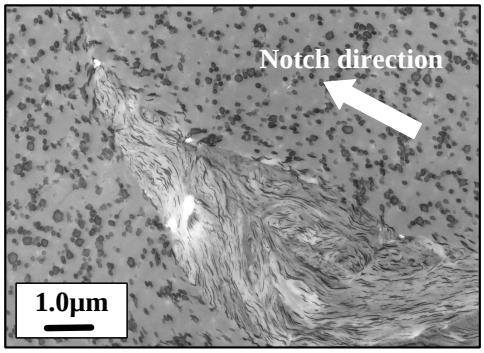

Figure 4: Plastic deformation in MBS resin.

A TEM micrograph of micro-deformation in a crack-tip region is shown in Figure 4. The deformation zone formed a kind of wedge shape, and large scale plastic deformation of the particles and surrounding matrix is observed within the zone. It is presumed that this kind of plastic deformation is created by solidification after flow process due to heat generation above glass transition temperature. It is noted that this type of deformation was not observed in the crack-tip region of the DENB specimen tested at a quasi-static loading-rate. It is therefore concluded that the high stress concentration in crack-tip region under high strain-rate condition results in such flow-like plastic deformation. Heat generation in crack-tip region of polymer has been studied theoretically and experimentally [4-7].

3 FINITE ELEMENT ANALYSIS

3.1 Macro-scale model

The macro-scale model was developed on the basis of the half of the specimen geometry to simulate the damage zone formation shown in Fig.1. The FEA model is shown in Figure 5. FEMAP and MENTAT were used as the pre and post processors, respectively. A commercial FEA code, MSC/Marc, was used for this analysis. Plane stress condition was assumed, and 2126 of 6-node triangle elements were used to construct the half of the specimen. A damage model was introduced in this analysis to express the stiffness reduction due to macro-scopic damage zone formation. In an element, if the maximum principal stress reaches the critical value of damage formation, then the stiffness of the element in the principal stress direction decreases. For compressive stress, there is no such stiffness reduction. The elastic modulus and the Poisson's ratio were assumed to be 2.6 GPa and 0.35 from experimental results, respectively. The critical stress of damage formation was chosen as 50 MPa, and the softening modulus which is the slope of the tensile stress-strain curve after damage formation was 25 MPa.

In this analysis, the damage zone can be expressed as the region where extra-strain, called equivalent damage strain, is generated due to damage formation. Distribution of equivalent damage strain in the notch-tip region is shown in Figure 6. The damage region extends in the notch direction, and this result is similar to the damage zone formation shown in Fig.1.

3.2 Micro-scale model

A micro-scale model in which rubber particles are distributed in matrix was developed to simulate micro-craze formation in the surroundings of the particles. The model is shown in Figure 7. A FE-SEM micrograph of the microstructure was used to develop this model, and the edge length is equivalent to 210 μm. 5804 of 3-node plane-strain triangle elements were used to construct the

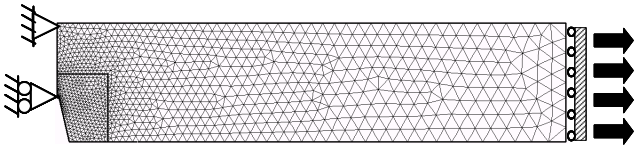

Figure 5: The macro-scale model.

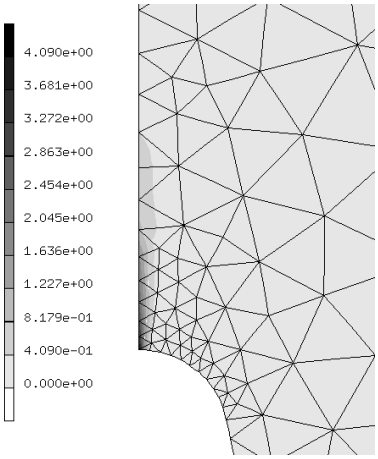

Figure 6: Equivalent damage strain distribution

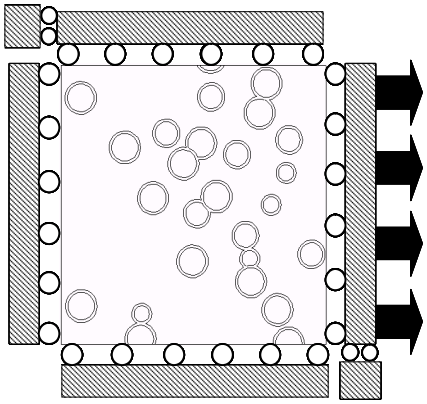

Figure 7: Micro-scale model.

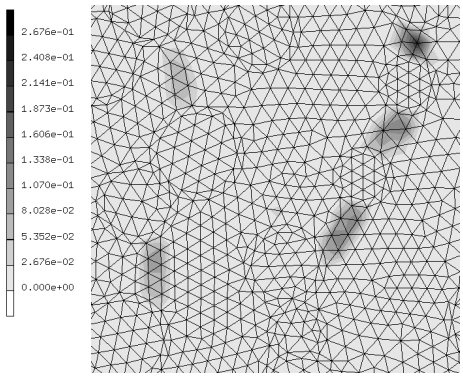

Figure 8: Distribution of equivalent damage strain.

model. The elastic modulus and Poisson's ratio were 3.34 GPa and 0.35 for PMMA matrix, and 1 MPa and 0.49 for rubber particles, respectively. The damage model described in the previous section was utilized to simulate micro-craze formation. The critical stress of craze formation was chosen as 70 MPa. It was assumed that the tensile and shear stresses are transferred at the point where craze is formed.

The FEA result is shown in Figure 8. The damage regions are initiated from the equators of the particles, and their directions of growth are almost perpendicular to the tensile direction shown in Fig.8. This corresponds to the growth behavior of micro-crazes observed by TEM shown in Fig.2.

3.3 Heat generation analysis

The half of SENB specimen was modeled in the FEA of the MBS resin. The SENB specimen model is shown in Figure 9. Loading part was assumed to be a circular steel ball of 2mm radius that is equivalent to the radius of the loading dart of the instrumented drop weight testing

apparatus. A load-displacement relation obtained from an impact fracture test of the MBS resin was given as the boundary condition for the steel ball. It takes 1.5 ms until the displacement reaches its maximum value 0.75 mm. FEMAP and LS-DYNA were used as the preprocessor and solver, respectively. The finite element mesh is shown in Figure 10. 4-node plane strain elements were used, and the numbers of element and node were 1502 and 1638, respectively, and the minimum size of element was 1.7 μm. A simple elastic-plastic model in which the nonlinear stress-strain curve is expressed by two linear lines was used as the constitutive model. Elastic strain energy stored in the elements plastically deformed was assumed to be transformed into thermal energy. In general, some of the material constants of thermoplastics strongly depend upon temperature; therefore, in this analysis, the elastic modulus, E_d, yield strength, σ_y, and work hardening parameter, E_t, were assumed to be temperature-dependent. The three parameters are shown in Table 1, and the basic material constants are shown in Table 2.

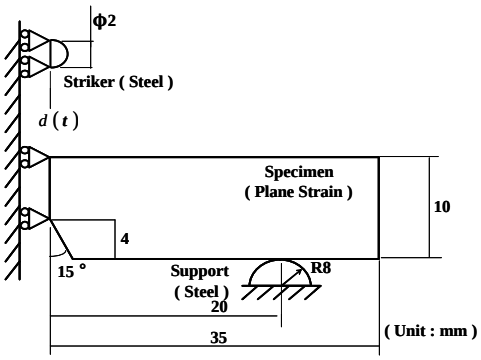

Figure 9: SENB specimen model.

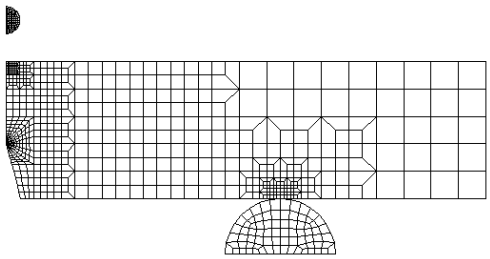
Figure 10: Finite element mesh.

Table 1 : Temperature-dependent material constants.

T (°C)	E_d (GPa)	σ_y (MPa)	E_t (MPa)
20	3	75	300
25	3	75	300
50	2	62	200
75	1	38	100
90	0.4	17	40
100	0.01	1	1

Table 2 : The basic material constants.

Material	E_d (GPa)	σ_y (MPa)	ν_d	E_t (MPa)	ρ (kg/m^3)	C (cal/g°C)	H (W/mK)	α (1/°C)
MBS	3	75	0.28	300	1050	0.38	0.2	7.4×10^{-5}
Steel	206	?	0.3	?	7860	0.072	30	?

Temperature distribution at the maximum displacement 0.75 mm is shown in Figure 11. It is seen that heat generation took place in the limited small region in the vicinity of the notch-tip. The maximum temperature was about 80°C. Another analysis conducted using only the basic constants that are independent of temperature showed that the maximum temperature was 58°C. Thus, the

temperature-dependence of the material constants tends to rise the maximum temperature, corresponding to increase of elastic strain energy during plastic deformation. It is known that the glass transition temperature of typical MBS resin is about 80-100ºC. Hence, the present analysis successfully exhibited the possibility of heat generation which may cause flow-like deformation in notch-tip region shown in Fig.4 in the MBS resin. For polymeric materials, it is known that some part of energy spend for plastic deformation and/or craze formation can be transformed into thermal energy. Therefore, if a new heat generation model considering the transformation from plastic to thermal energy in addition to the current elastic-thermal transformation is included in this FEA, generation of higher temperature at the notch-tip will be able to be simulated.

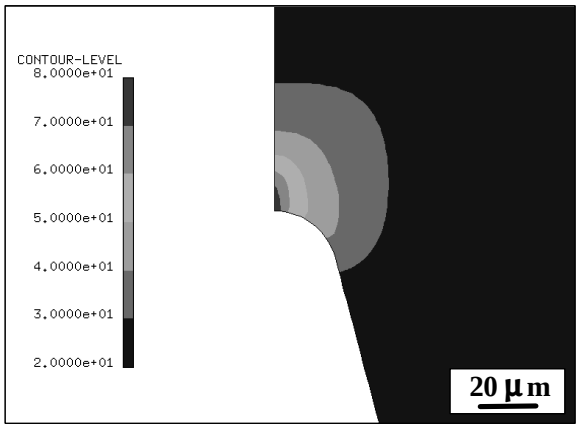

Figure 11: Temperature distribution in notch-tip region.

4 CONCLUSION

In-situ observation of damage zone formation in RT-PMMA was conducted, and a nonlinear FEA with the aid of a damage model was then performed to simulate such phenomenon in notch-tip region. The damage zone development was successfully simulated using the macro-scale modeling. The micro-scale model consisting of distributed rubber particles and matrix was also developed to analyze micro-craze formation in the surroundings of the particles. The FEA result exhibited good correlation with the initiation and growth behavior of mciro-crazes observed by TEM. Nonlinear dynamic FEA was also performed to simulate heat generation in MBS resin. The maximum temperature at the notch-tip obtained from the FEA was very close to the glass transition temperature of MBS, suggesting the possibility of flow-like deformation in notch-tip region.

REFERENCES

1. Todo, M., Takahashi, K., Beguelin, Ph., and Kausch, H.H., JSME Inter. J., Series A, 42-1 (1999), 49-56.
2. Todo, M., Takahashi, K., Jar, P.-Y.B., Beguelin, Ph., JSME Inter. J., Series A, 42-4 (1999), 585-591.
3. Todo, M., Arakawa, K., Takahashi, J., and Watanabe, H., Reports of RIAM Symposium, No.15ME-S1, 2004, 85-88.
4. Williams, J.G., Inter. J. Frac. Mech., 8-4 (1972), 393-401.
5. Doll, W., Eng. Frac. Mech., 5 (1973), 259-268.
6. Tomashevskii, E.E., Egorov, E.A., and Savostin, A.Y., Inter. J. Frac., 11-5 (1975), 817-827.
7. Fuller, K.N.G., Fox, P.G., and Field, J.E., Proc. R. Soc. Lond., A. 341 (1975), 537-557.